COMMUNICATION

An antibacterial conjugate of carbon nanohorns for NIR-light mediated peri-implantitis treatment †

Received 00th January 20xx,
Accepted 00th January 20xx

DOI: 10.1039/x0xx00000x

Eri Hirata[*a], Yuta Takano[*b,c], Daisuke Konishi[a], Yukari Maeda[a], Natsumi Ushijima[d], Masako Yudasaka[e,f] and Atsuro Yokoyama[a]

This study developed a novel antibacterial conjugate based on carbon nanohorns for peri-implantisis, an inflammatory disease around dental implants, which may result in failing implants by bone loss around them. The conjugate demonstrates much better photodurability than commonly used Indocyanine Green and a significant antibacterial effect under NIR illumination.

Carbon-based nanomaterials have attracted significant attention due to their unique chemical and physical properties.[1] Carbon nanomaterials, including carbon nanotubes, fullerenes, carbon nanohorns (CNHs), and graphene, have been extensively studied for their unique properties and potential applications in various fields, particularly biomedical fields.[1,2] These materials have great potential in drug delivery systems, tissue engineering, biosensors, and other biomedical applications.

Among the carbon nanomaterials, the large surface area and spherical morphology of CNHs offer their bio-functionality and biocompatibility.[3,4] Our research group has explored and reported potential applications of CNHs-modified titanium oxide to dental implants.[5,6]

Dental implant treatments are highly predictable for missing teeth.[7] However, peri-implantitis is a severe problem that can lead to implant loss. The inflammation of the mucous tissue around implants affects the connective tissue and bone, resulting in the loss of supporting bone around the implant. Roccuzzo et al. reported that the incidence of peri-implantitis is 43% on average,[8] and Schwarz et al. reported that the 10-year incidence of peri-implantitis in the non-periodontitis group was 6%.[9] The most common cause of peri-implantitis is the bacteria, represented by *Aggregatibacter actinomycetemcomitance* (*A.a.*),[10,11] adhering to the implant surface.[8,12,13] Although severe peri-implantitis often causes implant loss, effective treatment methods have not been established.

Several approaches have been proposed for the treatment of peri-implantitis, including nonsurgical methods, surface decontamination, and surgical treatments.[14] Current implant surfaces are treated to promote bone integration. The complex three-dimensional surface structure makes it difficult to remove bacteria, limiting the success of most treatment modalities, including surgery.[15,16] One treatment for peri-implantitis is the topical administration of antibiotics. Because of the diverse microflora present in peri-implantitis lesions, broad-spectrum antibiotics are used. However, there is concern about allergic reactions and increased antibiotic resistance.[17–19] In this regard, photodynamic therapy (PDT) is considered a practical approach for oral treatment, including peri-implantitis, because light illumination is easily accessible to the affected area.[20,21]

Recently, near-infrared (NIR) light, particularly in the 700-1300nm range called the biological window,[22] is considered to be essential to achieve efficient PDT. Ultraviolet and visible lights are absorbed and scattered by the surface of biological tissue, making it difficult to reach deep areas. Reaching deep pockets is vital for treating peri-implantitis in the submucosal tissue. Although there are several reports on NIR-PDT to cure peri-implantitis based on the elimination of the pathogen, mainly *A.a.*, all examples used Indocyanine Green (ICG) combined with an NIR laser[23], to our best knowledge. ICG is not stably decomposed during the prolonged illumination,[24] and thus higher or repeated doses are generally required for the treatment with injection or surgery. Therefore, it is desired to develop NIR-PDT reagents that require less frequent and less invasive administration.

In this study, we develop antibacterial conjugates of CNHs and an NIR-photosensitizer, π-extended porphyrin-type photosensitizer (**rTPA**),[25,26] towards an effective peri-implantitis therapy. **rTPA** generates singlet oxygen ($^1O_2$) from oxygen molecules under the NIR light irradiation. Especially, we aim *A.a.*

[a] *Department of Oral Functional Prosthodontics, Graduate School of Dentistry, Hokkaido University Sapporo 060-8586, Japan.*
E-mail: erieri@den.hokudai.ac.jp
[b] *Research Institute for Electronic Science and Graduate School of Environmental Science, Hokkaido University, Kita-20, Nishi-10, Sapporo 001-0020, Japan.*
E-mail: tak@es.hokudai.ac.jp
[c] *Graduate School of Environmental Science, Hokkaido University, N10, W5, Sapporo 060-0810, Japan.*
[d] *Support Section for Education and Research, Faculty of Dental Medicine, Hokkaido University, Sapporo 060-8586, Japan*
[e] *Nanomaterials Research Institute (NMRI), National Institute of Advanced Industrial Science and Technology (AIST), Tsukuba Central 5, 1-1-1 Higashi, Tsukuba, Ibaraki 305-8565, Japan.*
[f] *Meijo University, Graduate School of Science and Technology 1-501, Shiogamaguchi, Tenpaku, Nagoya 468-8502, Japan.*
† Electronic Supplementary Information (ESI) available: [details of any supplementary information available should be included here]. See DOI: 10.1039/x0xx00000x

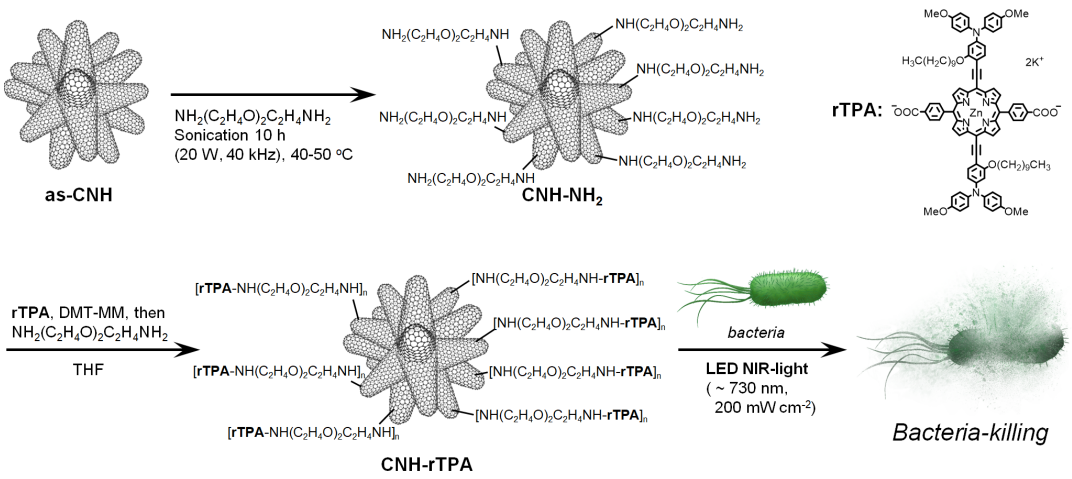

Scheme 1. Synthetic scheme of the conjugates (**CNH-rTPA**) of CNH and the NIR-photosensitizer (**rTPA**), and NIR-light induced bacteria-killing.

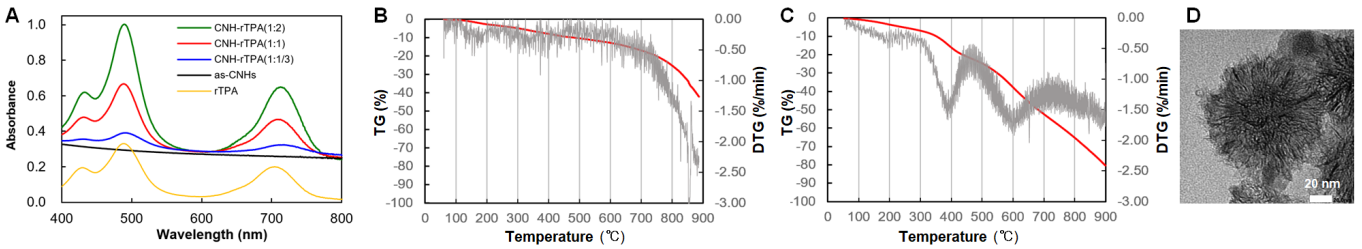

Fig. 1 (A) Absorption spectra of as-grown CNH (**as-CNH**), **rTPA**, and **CNH-rTPA** in PBS, where the concentration of CNHs were identical to be 1.00 μg mL^{-1}. Thermogravimetric (TG) and differential TG (DTG) data for (B) **CNH-NH$_2$**, and (C) **CNH-rTPA(1:1)** specimens, and (D) TEM image of **CNH-rTPA** by HAADF-STEM (80 kV).

as the target pathogen because the bacteria is considered as the main pathogen and possess unique selectivity toward drugs.[10,11] We anticipated that the CNH acts as an excellent scaffold because of its biocompatibility, potential ability in bone-engineering,[5,6,27] and well-fixation and alignment of the photosensitizer molecules. **rTPA** demonstrated the effective generation of $^1O_2$ under NIR illumination.

The **CNH-rTPA** was prepared by an amide-condensation of **CNH-NH$_2$** and the carboxylic group of **rTPA** using DMT-MM as the condensation reagent (Scheme 1). The aminated CNH (**CNH-NH$_2$**) was readily synthesized from as-grown CNH (**as-CNH**) by the simple method using sonication developed by E. Miyako and co-workers[28]. Three compositions of samples were prepared by changing the weight ratio of CNHs to **rTPA** by 1.00:0.33, 1.00:1.00, and 1.00:2.00 (w/w) (labeled as **1:1/3**, **1:1**, or **1:2**, respectively hereafter) for examining the introduced amount-dependent effect from **rTPA**. An excess amount of the diamine ($NH_2(C_2H_4O)_2C_2H_4NH_2$) was added to quench the reaction, and therefore **rTPA** molecules were introduced onto CNHs multiply. The free **rTPA** molecules and reaction byproducts were removed by filtration through a 0.2 μm PTFE filter. The target compound **CNH-rTPA** was obtained on the filter paper as their sizes, which were confirmed by DLS measurements (See supporting information, Fig. S1), are larger than 0.2 μm.

Successful coupling of **rTPA** with **CNHs-NH$_2$** was confirmed by UV-vis-NIR spectra, infrared (IR) spectra, and thermogravimetric analyses (TGA). Optical absorption spectra of **CNH-rTPA(1:1/3)**, **CNH-rTPA(1:1)**, and **CNH-rTPA(1:2)** clearly showed broad absorption of CNHs in the vis-NIR region and the characteristic peaks from **rTPA** (480 and 712 nm), which slightly shift from pristine **rTPA** (489 and 704 nm) (Fig. 1A). This result indicates that CNH effectively distributes rTPA moieties on its surface, preventing unwanted molecular aggregation that leads to severe band shifting, broadening, and reduced photoactivity of **rTPA**.[29] The comparable peak wavelengths of the three **CNH-rTPA** samples indicate almost the same electronic properties derived from **rTPA** in them. The peak areas derived from **rTPA** for **CNH-rTPA(1:1/3)**, **CNH-rTPA(1:1)**, and **CNH-rTPA(1:2)** are proportional to the introduced amounts of **rTPA** to the samples. Assuming that the absorption coefficient of **rTPA** in PBS (ε = 4.11 × 10^3 mol L^{-1} at 704 nm, Fig. S2) can be applied to the peak intensity of **CNH-rTPA**, although some error and underestimation may occur, the amount of porphyrin on 1.0 mg of CNHs was determined to be 0.19, 0.80 and 1.5 mg for **CNH-rTPA(1:1/3)**, **CNH-rTPA(1:1)**, and **CNH-rTPA(1:2)**, respectively. These correspond to 6.9 × 10^{16}, 2.9 × 10^{17}, and 5.5 × 10^{17} molecules per 1.0 mg of CNHs.

IR spectra support the success of the amide condensation. As a representative IR spectrum, **CNH-rTPA(1:1)** demonstrated the characteristic peaks of **rTPA** originated from the triple bonds (2172 cm^{-1}) and the aromatic rings (1592 and 1497 cm^{-1}) (Fig. S3). The shift of C=O of **rTPA** from 1697 to 1650 cm^{-1} in **CNH-rTPA(1:1)** indicates the formation of the amide bond between **CNHs-NH$_2$** and **rTPA**.

TGA analyses further confirm the successful attachment of **rTPA** on **CNHs-NH$_2$**. **rTPA** demonstrates a differential peak of

weight loss around 400 °C (Fig. S2). **CNH-rTPA(1:1)** demonstrated the corresponding characteristic peak around 400 °C, whereas pristine CNHs and **CNH-NH$_2$** do not show such a peak (Figs. 1B, 1C and S4). A new peak around 600 °C in **CNH-rTPA(1:1)** would be attributed to the **rTPA** located near the core of CNHs, which can be relatively stable against heating.[30] A similar kind of higher-temperature shift because of the stabilization was reported for CNHs and minocycline conjugate due to the π-π interaction.[30] TEM observations confirmed the morphology of the sample. A characteristic dahlia-shaped structure was observed in **CNH-rTPA(1:1)** (Fig. 1D). This result indicates that the original structure of CNHs is maintained after the amide-condensation reaction (Fig. 1D and S5).

The photostability of **CNH-rTPA** under NIR light was examined (Fig. 2). **CNH-rTPA(1:1)** and pristine **rTPA** did not show photo-bleaching, while ICG, which is commonly used for NIR-PDT recently, demonstrated significant bleach up to 69% of fade after 15 min illumination. This result indicates that **CNH-rTPA** has a high advantage over ICG in terms of photodurability.

$^1O_2$ generation abilities were examined on **CNH-rTPA(1:1/3)**, **CNH-rTPA(1:1)**, and **CNH-rTPA(1:2)**. $^1O_2$ which is produced by the photoenergy transfer from a photosensitizer plays a main role in the bactericidal effect. To fairly assess the ability of **CNH-rTPA** to produce $^1O_2$, the absorbances derived from the rTPA moiety in each sample were made identical. Not like previous reports using NIR-laser light[23], 730 nm LED light was employed to illuminate the sample solutions. The use of LED light is an advantage of the present study over previous studies because it is not expensive, and UV and visible LEDs are already approved for dental treatments in many countries.[31] Among the three **CNH-rTPA** samples, **CNH-rTPA(1:1)** showed the highest ability to generate $^1O_2$, probably due to a good balance in the amounts of **rTPA** and CNHs (Fig. 3A). Noteworthy, the physiological PBS solution of **rTPA** did not show significant $^1O_2$ generation, probably due to the aggregation of rTPA caused by the high ionic strength. This result suggests that the CNH acts as a good scaffold to distribute rTPA moieties on the surface, avoiding undesired molecular aggregation.

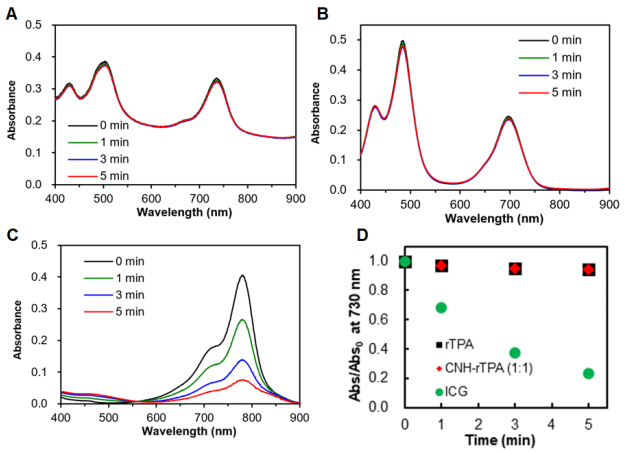

Fig. 2 Absorption spectra of (A) **CNH-rTPA(1:1)**, (B) **rTPA**, and (C) Indocyanine Green (ICG) with the illumination of 730 nm LED light (400 mW cm^{-2}). The absorbances of the dye molecules of the three compounds are identical at 0 min at 730 nm. (D) The time courses of the normalized absorbance at 730 nm for the samples in Fig. 2A-C

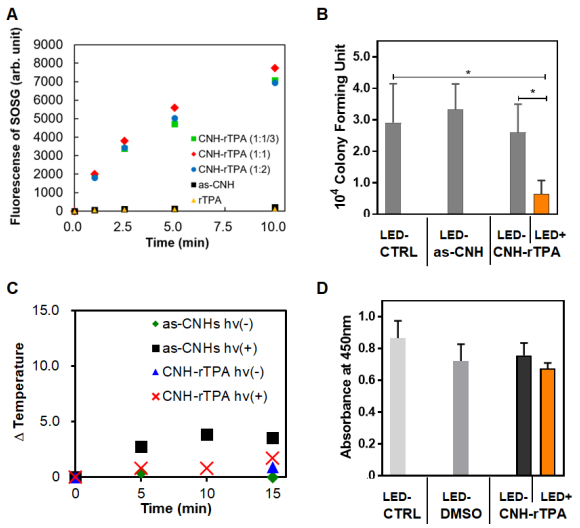

Fig. 3 (A) Singlet oxygen generation abilities of **CNH-rTPA**, **as-CNH**, and **rTPA** under the illumination by a 730 nm LED light (200 mW cm^{-2}). (B) NIR photo-induced bactericidal effect on *Aggregatibacter actinomycetemcomitance* (*A.a.*), (C) temperature rise of solution in a well of a 96-well plate, and (D) WST-1 assay on NIH/3T3 cells to verify no cytotoxicity under the illumination by a 730 nm LED light (400 mW cm^{-2}, 5 min). Statistically significant differences between that with and without illumination is illustrated with asterisks (*P < 0.05), and data without symbols are not significantly different p > 0.05 compared to the negative conditions (CTRL).

As **CNH-rTPA(1:1)** showed the best performance to generate $^1O_2$, it was focused for investigating the PDT effect on bacteria. **CNH-rTPA(1:1)** was added to a suspension of *A.a.* and then irradiated by the 730 nm LED. After the irradiation, the number of colonies decreased markedly by 35% compared to without irradiation, as shown in Fig. 3B. The condition of **as-CNH** alone did not result in any changes in colony numbers. The temperature of the medium containing **CNH-rTPA(1:1)** increased less than 2°C after the irradiation (Fig. 3C), suggesting the bactericidal effect was predominantly exerted by the generation of $^1O_2$ rather than the photothermal effect.

To verify its cytocompatibility, fibroblast cells, NIH/3T3, were cultured with **CNH-rTPA(1:1)**, for 4 hours and irradiated by the NIR light. The cells were then cultured for another 24 hours, and the cell numbers were evaluated by the WST-1 assay. As a result, no dramatic decrease in cell viability was observed (Fig. 3D). Therefore, it was concluded that exposure to **CNH-rTPA(1:1)** and its bactericidal PDT effect have minimal effects on the proliferation of fibroblast cells.

Several studies have been conducted on PDT using nanocarbons containing CNH[32,33]. Graphene has also been used to modify the surface of implants to provide antimicrobial activity[34,35]. On the other hand, there is a lack of research on applying NIR light to PDT for treating peri-implantitis. When surface treatments with antimicrobial activity are applied, the desorption of the coating layer during and after implant placement and the persistence of antimicrobial activity are unknown. This study aimed to apply **CNH-rTPA** to PDT, in which **CNH-rTPA** is injected into the peri-implantitis-affected area and irradiated with near-infrared light to eliminate bacteria. Compared to the previous PDT, which uses relatively short wavelengths and has limited penetration depth, our approach using NIR light could penetrate mucosal tissue and effectively

treat contaminated implant surfaces. Furthermore, since **CNH-rTPA** is 100-200 nm in diameter (Figs. S1 and S5), it could remain on the micro- and nanostructured surfaces of implants.

In the present study, we have developed an NIR-PDT reagent that can effectively treat the pathogen of peri-implantitis without causing deleterious effects *in vitro*. The simplicity and cost-effectiveness light source of this method make it a promising alternative to conventional treatment methods in the treatment of peri-implantitis.

Acknowledgments

We acknowledge Prof. T. Nakamura for using the TGA, financial support from MEXT under the JSPS KAKENHI (20K10025 and 23K09266 to E.H., 22K19609 to A.Y. and 21H01753 to Y.T.), the JSPS Core-to-Core Program for Advanced Research Network, the JSPS Cooperative Research Program of "NJRC Mater. & Dev.", and Kao Foundation for Arts and Sciences.

Conflicts of interest

There are no conflicts to declare.

Notes and references

1 S. Iijima, M. Yudasaka, R. Yamada, S. Bandow, K. Suenaga, F. Kokai and K. Takahashi, *Chem. Phys. Lett.*, 1999, **309**, 165–170.

2 Z. Peng, T. Zhao, Y. Zhou, S. Li, J. Li and R. M. Leblanc, *Adv. Healthc. Mater.*, 2020, **9**, 1901495.

3 M. Zhang, M. Yang, C. Bussy, S. Iijima, K. Kostarelos and M. Yudasaka, *Nanoscale*, 2015, **7**, 2834–2840.

4 B. He, Y. Shi, Y. Liang, A. Yang, Z. Fan, L. Yuan, X. Zou, X. Chang, H. Zhang, X. Wang, W. Dai, Y. Wang and Q. Zhang, *Nat. Commun.*, 2018, **9**, 2393.

5 E. Hirata, E. Miyako, N. Hanagata, N. Ushijima, N. Sakaguchi, J. Russier, M. Yudasaka, S. Iijima, A. Bianco and A. Yokoyama, *Nanoscale*, 2016, **8**, 14514–14522.

6 S. Takada, E. Hirata, M. Sakairi, E. Miyako, Y. Takano, N. Ushijima, M. Yudasaka, S. Iijima and A. Yokoyama, *Artif. Cells, Nanomedicine, Biotechnol.*, 2021, **49**, 20–29.

7 V. Moraschini, L. A. D. C. Poubel, V. F. Ferreira and E. D. S. P. Barboza, *Int. J. Oral Maxillofac. Surg.*, 2015, **44**, 377–388.

8 A. Roccuzzo, A. Stähli, A. Monje, A. Sculean and G. E. Salvi, *J. Clin. Med*, 2021, 10.

9 F. Schwarz, J. Derks, A. Monje and H. L. Wang, *J. Clin. Periodontol.*, 2018, **45**, S246–S266.

10 J. Sun, J. Eberhard, S. Glage, N. Held, H. Voigt, K. Schwabe, A. Winkel and M. Stiesch, *Clin. Oral Implants Res.*, 2020, **31**, 203–214.

11 M. Albertini, L. López-Cerero, M. G. O'Sullivan, C. F. Chereguini, S. Ballesta, V. Ríos, M. Herrero-Climent and P. Bullón, *Clin. Oral Implants Res.*, 2015, **26**, 937–941.

12 R. Smeets, A. Henningsen, O. Jung, M. Heiland, C. Hammächer and J. M. Stein, *Head Face Med.*, 2014, **10**, 34.

13 J. B. Suzuki, L. D. Terracciano-Mortilla and C. E. Misch, *Dent. Implant Prosthetics*, 2015, 964–981.

14 D. Rokaya, V. Srimaneepong, W. Wisitrasameewon, M. Humagain and P. Thunyakitpisal, *Eur. J. Dent.*, 2020, **14**, 672–682.

15 G. Baima, F. Citterio, M. Romandini, F. Romano, G. M. Mariani, N. Buduneli and M. Aimetti, *Clin. Oral Implants Res.*, 2022, **33**, 1069–1086.

16 Y. C. M. De Waal, | Lewis Winning, | Andreas Stavropoulos and I. Polyzois, *J Clin Periodontol*, 2022, 1–12.

17 M. Feres, R. Martins, J. G. S. Souza, M. Bertolini, V. A. R. Barão and J. A. Shibli, *Clin. Implant Dent. Relat. Res.*, 2023, 767–781.

18 H. Koo, R. N. Allan, R. P. Howlin, P. Stoodley and L. Hall-Stoodley, *Nat. Rev. Microbiol.*, 2017, **15**, 740–755.

19 M. Øen, K. N. Leknes, B. Lund and D. F. Bunæs, *BMC Oral Health*, 2021, **21**, 1–15.

20 K. Konopka and T. Goslinski, *J. Dent. Res.*, 2007, **86**, 694–707.

21 D. Schär, C. A. Ramseier, S. Eick, N. B. Arweiler, A. Sculean and G. E. Salvi, *Clin. Oral Implants Res.*, 2013, **24**, 104–110.

22 Z. Ma, F. Wang, W. Wang, Y. Zhong and H. Dai, *Proc. Natl. Acad. Sci.*, 2021, **118**, 1–8.

23 S. Pakarinen, R. K. T. Saarela, H. Välimaa, A. M. Heikkinen, E. Kankuri, M. Noponen, H. Alapulli, T. Tervahartiala, I. T. Räisänen, T. Sorsa and T. Pätilä, *Dent. J.*, 2022, **10**, 206.

24 W. Holzer, M. Mauerer, A. Penzkofer, R.-M. Szeimies, C. Abels, M. Landthaler and W. Bäumler, *J. Photochem. Photobiol. B Biol.*, 1998, **47**, 155–164.

25 Satrialdi, R. Munechika, V. Biju, Y. Takano, H. Harashima and Y. Yamada, *Chem. Commun.*, 2020, **56**, 1145–1148.

26 Satrialdi, Y. Takano, E. Hirata, N. Ushijima, H. Harashima and Y. Yamada, *Nanoscale Adv.*, 2021, **3**, 5919–5927.

27 T. Kasai, S. Matsumura, T. Iizuka, K. Shiba, T. Kanamori, M. Yudasaka, S. Iijima and A. Yokoyama, *Nanotechnology*, 2011, **22**, 065102.

28 E. Miyako, J. Russier, M. Mauro, C. Cebrian, H. Yawo, C. Ménard-Moyon, J. A. Hutchison, M. Yudasaka, S. Iijima, L. De Cola and A. Bianco, *Angew. Chemie - Int. Ed.*, 2014, **53**, 13121–13125.

29 N. C. Maiti, S. Mazumdar and N. Periasamy, *J. Phys. Chem. B*, 1998, **102**, 1528–1538.

30 Y. Maeda, E. Hirata, Y. Takano, N. Sakaguchi, N. Ushijima, A. Saeki, S. Kimura, K. Shibata, M. Yudasaka and A. Yokoyama, *Carbon N. Y.*, 2020, **166**, 36–45.

31 A. D. Wilder, S. C. Bayne, K. N. May, K. F. Leinfelder and D. F. Taylor, *J. Dent.*, 1991, **19**, 214–220.

32 E. Miyako, H. Nagata, K. Hirano, Y. Makita, K. Nakayama and T. Hirotsu, *Nanotechnology*, 2007, **18**, 475103.

33 H. E. Karahan, C. Wiraja, C. Xu, J. Wei, Y. Wang, L. Wang, F. Liu and Y. Chen, *Adv. Healthc. Mater.*, 2018, **7**, 1–18.

34 R. Malhotra, Y. M. Han, J. L. P. Morin, E. K. Luong-Van, R. J. J. Chew, A. H. Castro Neto, C. A. Nijhuis and V. Rosa, *J. Dent. Res.*, 2020, **99**, 285–292.

35 M. Gu, L. Lv, F. Du, T. Niu, T. Chen, D. Xia, S. Wang, X. Zhao, J. Liu, Y. Liu, C. Xiong and Y. Zhou, *Sci. Rep.*, 2018, **8**, 8141.

